

This manuscript has been authored by UT-Battelle LLC under Contract No. DE-AC05-00OR22725 with the U.S. Department of Energy. The United States Government retains and the publisher, by accepting the article for publication, acknowledges that the United States Government retains a non-exclusive, paid-up, irrevocable, world-wide license to publish or reproduce the published form of this manuscript, or allow others to do so, for United States Government purposes. The Department of Energy will provide public access to these results of federally sponsored research in accordance with the DOE Public Access Plan (<http://energy.gov/downloads/doe-public-access-plan>).

Reaction-bond composite synthesis of SiC-TiB₂ by Spark Plasma Sintering/Field-Assisted Sintering Technology (SPS/FAST)

Corson L. Cramer^{1,*}, Jake McMurray², Michael J. Lance², Richard A. Lowden²

¹Energy & Environmental Sciences Directorate, Oak Ridge National Laboratory, Oak Ridge, TN, USA

²Materials Science and Technology Division, Oak Ridge National Laboratory, Oak Ridge, TN, USA

*cramercl@ornl.gov

Abstract

High-density SiC-TiB₂ composites were fabricated using the displacement reaction spark plasma sintering/field-assisted sintering technology (SPS/FAST) and SiC, B₄C, TiC, and Si powders. The reaction process was performed in a narrow time frame compared hot pressing. The SiC-TiB₂ composites were sintered with precursor SiC at various pressures to determine the effects of processing with SPS/FAST. The composites completed synthesis during SPS/FAST processing, which occurs more quickly than hot pressing. SEM, STEM, and Raman spectroscopy are used to show the conversion and microstructure. The composite of 53.6 wt.% SiC and 46.4 wt.% TiB₂ has 99% theoretical density, hardness of 26.4 GPa, and fracture toughness of 5.12 MPa·m^{1/2}.

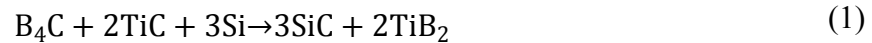
Key Words: Ceramic composites; reaction bonding; Spark plasma sintering

Introduction

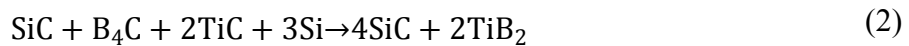
Silicon carbide (SiC) and titanium diboride (TiB₂) both have high melting points, high hardness, excellent chemical stability, and low density, which are highly desirable properties for armor, wear, and high-temperature applications [1]–[6]. However, it is not currently possible to synthesize dense objects of these compounds using solid-state processing methods due to their strong covalent bonding and low self-diffusion [7]. Making ceramic matrix composites (CMCs) is sometimes easier with these materials, so they are often processed as composites with phases such as alumina, which aids in liquid-phase sintering [8]. When combining the phases, the fracture toughness and high-temperature stability of the CMC material are both greatly enhanced further than SiC and TiB₂ individually. SiC and TiB₂ are an ideal CMC pair because the SiC helps increase oxidation resistance and TiB₂ helps increase fracture toughness [9]–[11]. These two components cannot be processed with liquid-phase sintering unless another material is added [12], so a different approach is needed. Reaction bonding of these two materials can create interconnect or matrix-type microstructure, and the approach usually involves reaction of precursors and displacement reactions.

The synthesis of SiC-TiB₂ composites has been done with hot pressing by reacting TiN and B in the presence of SiC particles [13]. Other precursors, such as TiH₂ [14] and Ti(C,N) [15], have been used to make reaction-bonded SiC-TiB₂, but the reactions involved produce unwanted by-products that hinder densification and reduce the mechanical properties. It has been shown that precursor powders of the B-Ti-C-Si system can form SiC-TiB₂ with no unwanted products and

full conversion to composite material [16]–[18]. SiC-TiB₂ composites have been processed with displacement reaction sintering in hot pressing of B₄C, Ti, and Si powders, but Ni was used to aid in the consolidation [19], [20]. The most consistent, pure, and highly dense reaction-bonded SiC-TiB₂ composites were processed with hot pressing B₄C, TiC, and Si precursor powders in the molar amounts of the reactants, as shown in Eq. (1) [21], [22]. In this displacement reaction, the B diffuses into the TiC and displaces C; the carbon is now free to form SiC with the Si. This does not happen at any reasonable time frame unless the Si is molten. The current research is based on the same chemistry and mechanisms.



Improvements to the reaction product can be made by varying both the processing and the materials. The processing of these materials can take time. A potentially faster method is spark plasma sintering/field-assisted sintering technology (SPS/FAST), which is a common technique used for materials processing [23]. Displacement reactions with SPS have been done with the TiC-TiB₂ composite system with micron-sized powders [24] and with the Ti₃SiC₂-SiC composite system with nanopowders [25]. Also, when more SiC is added, the oxidation resistance increased and density decreased, which aids in wear part and armor applications, respectively. The chemical reaction that takes place when SiC is added as a precursor is represented in Eq. (2).



In the current research, SPS/FAST processing was compared to literature available on hot pressing using B₄C, TiC, and Si powders as precursors so that a direct comparison can be made [21]. SiC was also added to the precursor powders used in previous hot-pressing studies, and the product was compared with that produced by SPS/FAST sintering without SiC. The effects of additional pressure on the density of the samples processed with SiC precursor was analyzed. It was found that processing time was significantly reduced when using SPS/FAST, compared to hot pressing. The theoretical density of a sample made from precursors containing added SiC is lowered because the product contains higher content of SiC, whose density is lower than that of TiB₂. The effects of composition and pressure on densification and chemistry were analyzed for the samples processed with SPS/FAST.

Materials and Methods

Boron carbide (B₄C) powder (Wacker Ceramics, 5 μm, LOT M193), TiC powder (PPM Ltd., 1–2 μm, 99.9%, stoichiometric), SiC powder (South Bay, 15 μm, 99.9%, stoichiometric), and –325 mesh Si powder (AEE, 99%) were used. The powders were mixed based on the stoichiometric amounts for the reactants in Eqs. (1) and (2). For samples processed according to Eq. (1), the amounts of precursor are 21.3 wt.% B₄C, 46.2 wt.% TiC, and 32.5 wt.% Si, which yields a final composite of 46.4 wt.% SiC and 53.6 wt.% TiB₂ and theoretical density of 3.80 g/cm³ based on the rule of mixtures. For samples processed according to Eq. (2), the amounts of precursors are 13.4 wt.% SiC, 18.5 wt.% B₄C, 40.0 wt.% TiC, and 28.1 wt.% Si, which yields a final composite

of 53.6 wt.% SiC and 46.4 wt.% TiB₂ and theoretical density of 3.71 g/cm³ based on the rule of mixtures. The two powder blends were mixed in a Spex (8000M) mill for 10 min with a duty cycle of 10%. The powders were loaded into 20 mm diameter graphite dies, and pressure was applied to an initial load of 10 MPa. The sintering was done in a Thermal Tech. Inc. SPS machine. All samples were heated to 1,700°C at a heating rate of 100°C/min and were held under a vacuum of 3×10^{-3} Torr for 10 min, which is almost ten times faster than hot pressing. Additional pressure was added to the composites containing precursor SiC to test the effects of pressure on densification. Table 1 lists values of particle sizes and processing times used for both hot pressing and SPS/FAST processing to facilitate a direct comparison. The only change when using SPS/FAST compared to hot pressing is the faster heating rate and an induced electric field induced during the SPS/FAST [26].

Table 1: Powder sizes and time for processing for hot pressing versus SPS/FAST.

Type of processing	B ₄ C powder size (μm)	TiC powder size (μm)	Si powder (mesh)	Time to process (min)	Induced Electric Field (V/cm)
Hot pressing [21]	3	1–3	–200	250 min	0–0.1
SPS/FAST	5	1–2	–325	27 min	1–5 [26]

The specimen microstructures were analyzed with a Hitachi S4800 scanning electron microscope (SEM) in backscatter electron imaging mode. Geometric and Archimedes densities were measured when appropriate by measuring the part dimensions, dry mass, and submerged mass. Optical images were taken using a Keyence VHX-1000 system; computational stitching of the images was used to display full cross sections. Crystallographic phase composition was determined by x-ray diffraction (XRD) using a PANalytical X'pert diffractometer with Mo K-α radiation ($\lambda = 0.709319 \text{ \AA}$). The operating parameters were 40 kV and 40 mA, with a 2θ step size of 0.02. The XRD patterns were analyzed using the whole pattern fitting approach with the MDI Jade 2010 software database. Vickers hardness measurements were performed using an Instron Wilson-Wolpert Tukon Vickers 2100B apparatus under a 1.5 kgf load. Palmquist indentation fracture toughness is performed on the samples. Differential thermal analysis (DTA) was performed with a Netzsch STA 449 F3 Jupiter simultaneous thermal analyzer in an argon atmosphere to identify reactions during processing. DTA scans were performed at ambient pressure and at a lower heating rate (10°C/min) than those associated with SPS/FAST. Although these conditions are not an exact representation of the actual processing conditions, information provided by DTA is still of value to understand the mechanisms leading to the final phase composition of the material. Scanning transmission electron microscopy (STEM) samples were made using a Hitachi NB-5000 dual beam focused-ion beam. Energy dispersive x-ray spectroscopy (EDS) STEM imaging was conducted using a FEI Talos F200X Scanning Transmission Electron Microscope. Raman spectra were collected using a Dilor XY800 Raman microprobe with a Coherent Innova Ar ion laser operating at 5145 Å and 1 mW and a spot size of 1 micrometer.

Results

Figure 1 shows the XRD patterns of the samples processed with SPS/FAST and the starting SiC powder. All the peaks are labeled on the SiC powder and the sample processed without SiC precursor, while only the additional peaks are labeled in the samples processed with SiC precursor. The sample without SiC precursor sintered under 30 MPa of pressure is the best comparison to hot pressing studies, while the samples sintered with SiC precursor under pressures of 30 MPa, 45 MPa, and 60 MPa are a new addition in order to achieve full density with SPS/FAST. Within the resolution limits of the diffractometer, it was found that for all processing conditions there was a full conversion of the precursors into SiC-TiB₂. Since SPS/FAST achieved full conversion to SiC-TiB₂ in less time than hot pressing, the reactions occurred quickly enough to completion when using SPS/FAST. Full conversion to SiC-TiB₂ also occurred when SiC was added as a precursor and when additional pressure was added to the powder system. The particles used as precursors are comprised of α -SiC of both 4-H and 6-H. The SiC that formed during SPS/FAST is β -SiC. The only remnant of α -SiC in the samples with SiC precursors was 4-H, meaning that 6H converted to 4H during processing. The crystal structure of β -SiC and α -SiC is zinc blende and hexagonal, respectively. The two α -SiC polytypes are distinguished by their repeating unit where the 6-H has a longer repeating unit. The conversion of 6-H to 4-H during processing is most likely due to the 4-H having higher stability. The reason for β -SiC formation versus α -SiC formation is not well understood, but it is likely formed from free amorphous carbon that comes from the displacement reaction between B₄C and TiC [27].

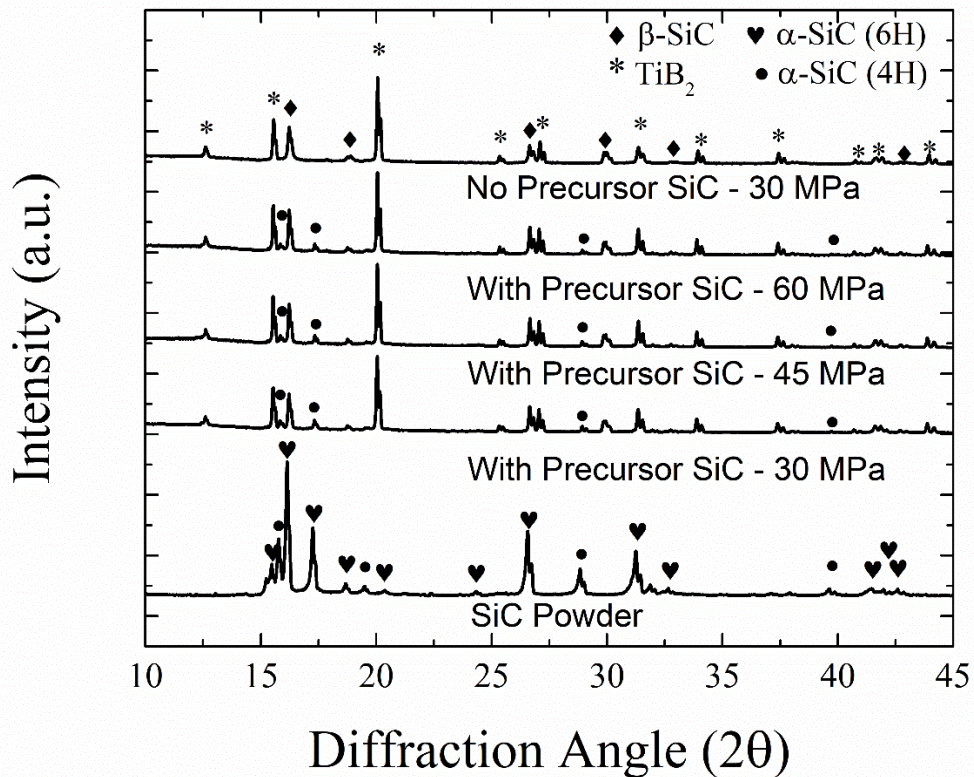


Figure 1: XRD scans of samples processed with SPS/FAST. Results are shown for samples processed with and without SiC as a function of pressure.

Figure 2 shows the DTA curves for the powder blends with and without precursor SiC. The exothermic direction is in the positive y -axis direction. A sharp endothermic peak at $1,414^{\circ}\text{C}$ on a DTA curve is usually associated with the melting of Si, but it is not present here. It has been shown that heating rate can affect the DTA data [28], so DTA of a heating rate as fast as SPS/FAST could help determine the reaction process, however, DTA systems are not set up for this. Also, the reactions and melting may be convoluted because all of the precursor materials are heated up together. The DTA data also show three broad peaks in the exothermic direction for both powder blends processed according to Eqs. (1) and (2). The peaks around 1050°C are most likely the solid-state displacement reactions between B_4C and TiC , and the peaks starting at 1550°C could be the reaction where Si in liquid phase transports boron (B) to free carbon forming TiB_2 or the formation of SiC [21]. The three peaks are not sharp, distinct reaction peaks, but the XRD indicates that the reactions occur. The reactions may proceed slowly, but they proceed to completion in the time frame associated with SPS/FAST according to XRD. At temperatures above 1400°C , samples processed with precursor SiC released less exothermic energy indicating that some of the SiC present in precursor absorbs some of the energy during the reaction.

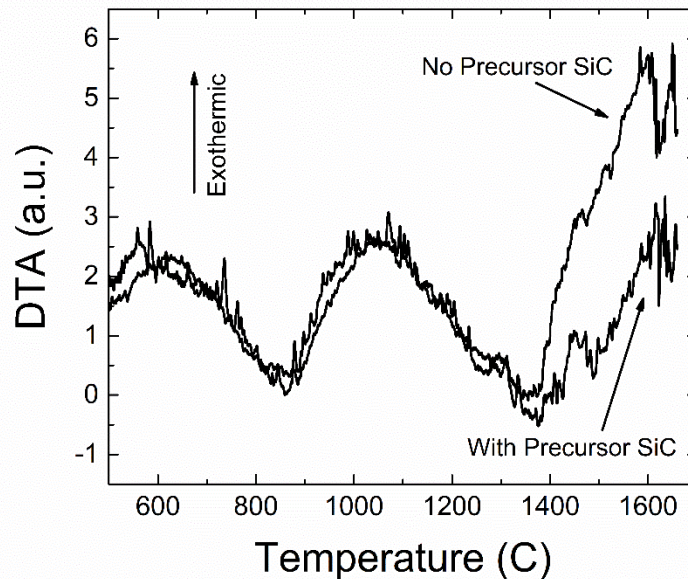


Figure 2: DTA data of the two different blends of B_4C , TiC , and Si with and without SiC.

Figure 3 shows densification curves for samples processed by SPS/FAST where the position of the rams in the SPS/FAST machine are monitored with a dilatometer as a function of the temperature. The position of the rams (mm) correlated to the compaction and consolidation of the powders, but since the composition was unknown at any given temperature because of reaction species, it was impossible to convert the displacement data to density data. All samples experienced shrinkage and densification up to $1,700^{\circ}\text{C}$, which was the hold temperature. The

final densities were measured and compared to the theoretical values based on the composite formation and rule of mixtures. The samples processed without SiC precursor and 30 MPa achieved a final density of 3.0 g/cm³, which is 80 % theoretical density (TD) based on a final composite density value of 3.8 g/cm³. The samples processed with precursor SiC had TD of 3.71 g/cm³. The samples processed with precursor SiC and 30 MPa reached final densities of 3.58 g/cm³, which is 95 %TD. The samples processed with precursor SiC and 45 MPa reached final densities of 3.62 g/cm³, which was 97 %TD. The samples processed with precursor SiC and 60 MPa reached final densities of 3.66 g/cm³, which was 99 %TD. These values can be seen in Table 2. The low density in samples processed without precursor SiC were not consistent with hot pressing, where the hot pressing of these powders and sizes achieved near-full density. This suggests the processing time frame and kinetics occur faster than the volume change or that one phase, either SiC or TiB₂, forms faster than the other. This may be from porosity and pore channel differences introduced from precursor particles, where the precursor yields favorable porosity and pore channels. It could also be that precursor SiC increases the electrical conductivity of the sample, which typically aids in sintering using SPS/FAST.

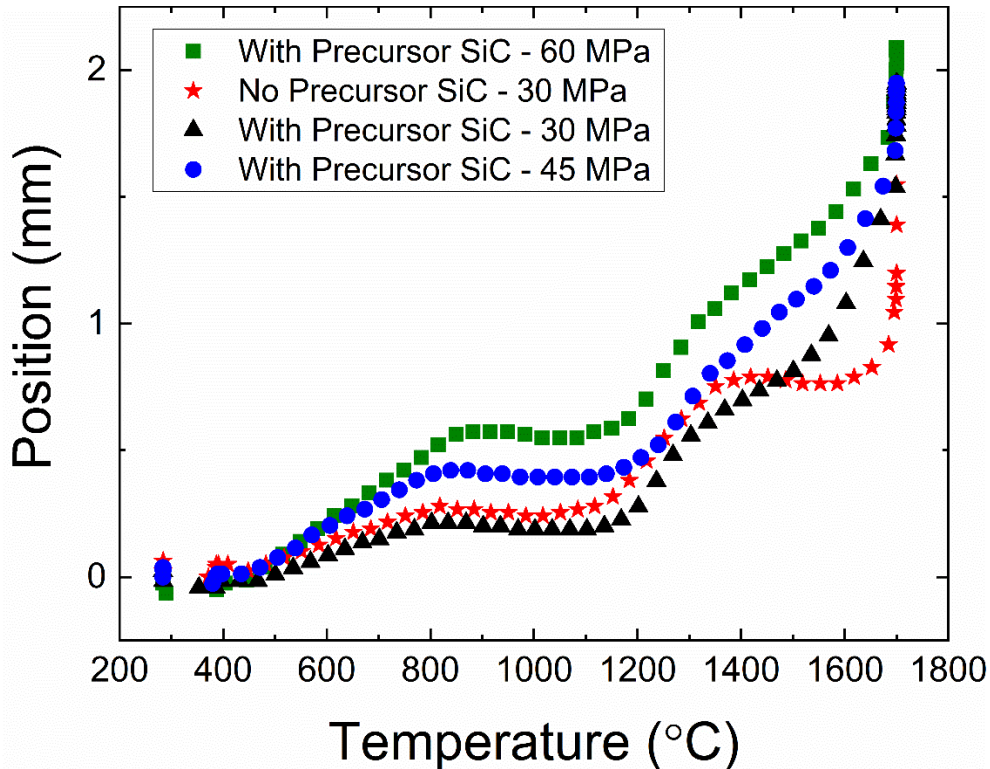


Figure 3: Densification curves of samples processed with SPS/FAST showing the change in position of the rams in the SPS/FAST machine, and thus compaction of the powder in mm, versus temperature.

Because the heating rates and compositions are similar for the SPS/FAST in the current research, there are most likely no changes in electric field for all samples processed, however, the samples with added precursor SiC change the conductivity of the overall electrical circuit, which includes the die/punches and the powders, and this could lead to increased joule heating. To investigate

the electrical changes during the processing, the resistance and power measured from the machine are presented. Figure 4 is a plot of the resistance and power as a function of temperature for samples processed at 30 MPa with and without precursor SiC. There is little difference in power when adding SiC when measuring from the machine, which includes both material and die/punches setup. The resistance, as measured through the machine, is slightly less when adding SiC. Thus, there is little no joule heating effects seen when adding SiC.

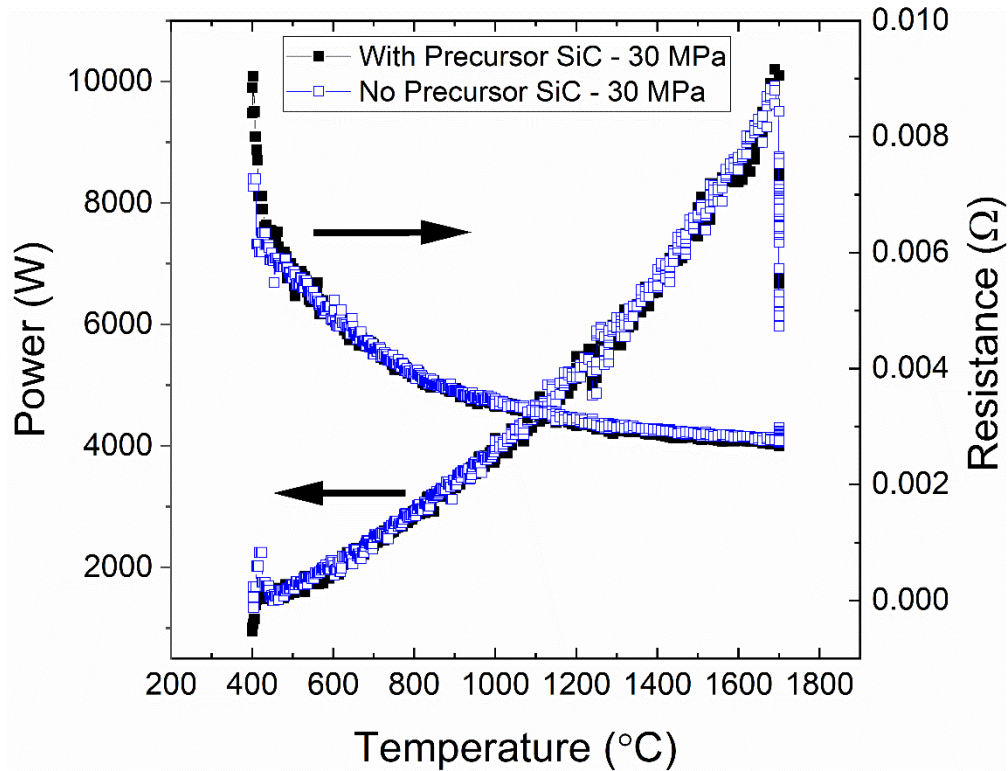


Figure 4: Power and resistance as a function of temperature for samples processed at 30 MPa with and without SiC precursor.

Figure 5 shows SEM images of the microstructures of the composite processed with no precursor SiC and 30 MPa in both backscatter and secondary electron mode. EDS data is not sensitive enough to detect B, but it helps differentiate the Si and Ti, thus the light grey phase marked with a circle is TiB_2 that formed during processing, and the dark grey phase within the TiB_2 marked with a star is SiC that formed during processing. The black areas are pores. Table 2 lists values of the composite densities, and this sample has a density of 80%TD.

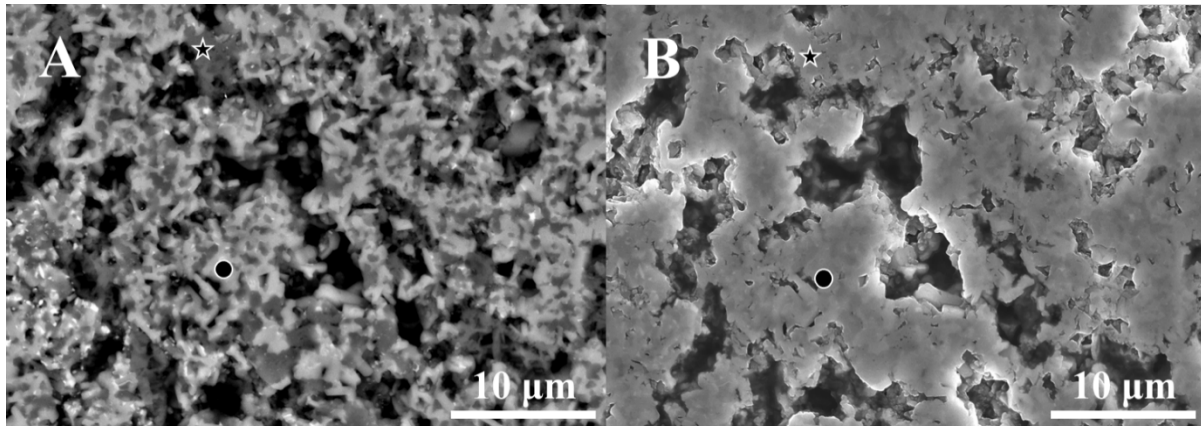


Figure 5: SEM images of the microstructure of the sample processed with no precursor SiC and 30 MPa in (A) backscatter mode and (B) secondary electron mode.

Figure 6 shows SEM images of the microstructures of the composite processed with precursor SiC and 30 MPa in both backscatter and secondary electron mode. In backscatter mode, the light grey phase marked with a circle is TiB_2 that formed during processing, and the dark grey phase is SiC. In backscatter mode, the difference in SiC is not apparent, so the secondary electron image is shown to differentiate the SiC precursor (marked by a square) and the SiC formed during processing (marked by a star). Some of the black-shaded areas are pores but not all, and the secondary electron image has better indication of pores. The density of the sample from Table 2 is 95%TD. The shade difference in the area where TiB_2 formed in a SiC matrix around the precursor SiC particles indicates that there might be a third phase present.

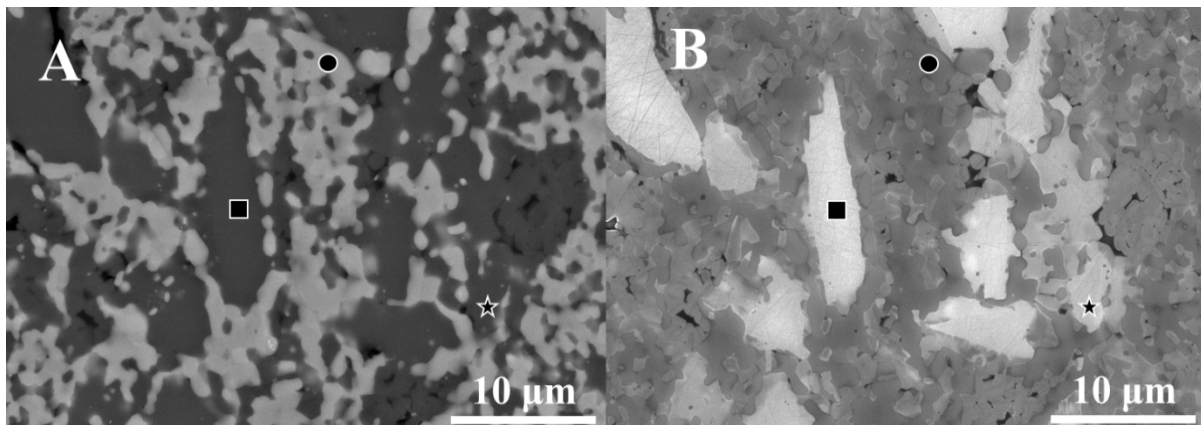


Figure 6: SEM images of the microstructure of the sample processed with precursor SiC and 30 MPa in (A) backscatter mode and (B) secondary electron mode.

Figure 7 shows SEM images of the microstructures of the composite processed with precursor SiC and 45 MPa in both backscatter and secondary electron mode. The microstructure and phases are very similar to the sample processed precursor SiC and 30 MPa, except the density of the sample from Table 2 is 97 %TD. Also, Figure 8 shows SEM images of the microstructures of the composite processed with precursor SiC and 60 MPa in both backscatter and secondary electron mode. The only difference is the density from Table 2 is 99 %TD. Again, there is a possible third phase present in these two samples.

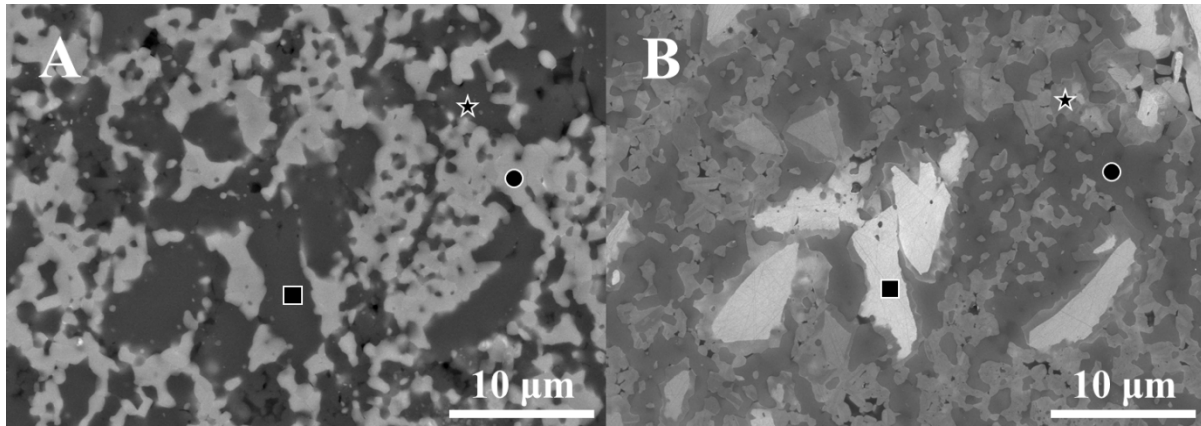


Figure 7: SEM images of the microstructure of the sample processed with precursor SiC and 45 MPa in (A) backscatter mode and (B) secondary electron mode.

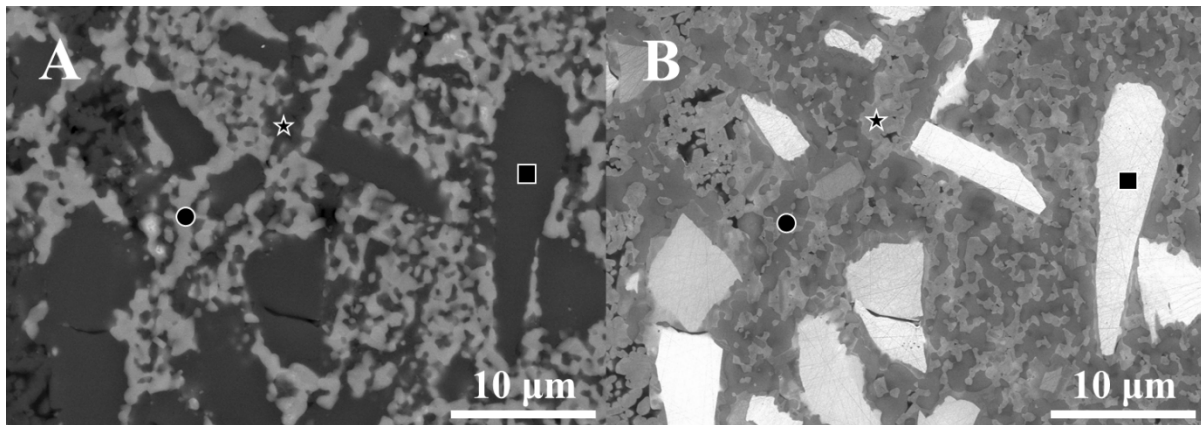


Figure 8: SEM images of the microstructure of the sample processed with precursor SiC and 60 MPa in (A) backscatter mode and (B) secondary electron mode.

To identify a possible third phase in the SiC-TiB₂ formed around the precursor SiC particles, further investigation was done on the sample processed with precursor SiC and 60 MPa. EDS with the SEM is not done because the B sensitivity is not good enough for mapping to the SEM image. To further identify the phases and understand the microstructure, STEM and EDS was done. Figure 9 shows the Dark Field STEM image, elemental mapping, and pole figure diagrams of the phases. The STEM image shows where the TiB₂ was formed in a SiC matrix. The image shows the twinning stacking fault line in the SiC, which is very common. From the EDS maps, it was shown that Ti and B are present in the same spot indicating TiB₂. Also, the Si and C show where the SiC is located. The two phases are distinct and very separate from each with intimate interfaces. The two phases are also crystalline as indicated by the pole figures. Also, the TiB₂ has seemed to pick up more oxygen compared to the SiC. There is a small spot, labeled using red arrows, that consists of Ti, B, and C, and is most likely some unreacted material. It could be TiC or B₄C, but further analysis of that phase is done with Raman Spectroscopy. Also, there is a small amount of another phase, which is mapped with Al and O. This phase is possibly some aluminosilicate that is amorphous, as indicated by the pole figure. Because the TiB₂ shows up with different shades in the SEM and STEM, the possible, unidentified phase in the SEM images

is different orientations of the TiB_2 . The amorphous Al-Si-O phase is too small to be seen in the SEM.

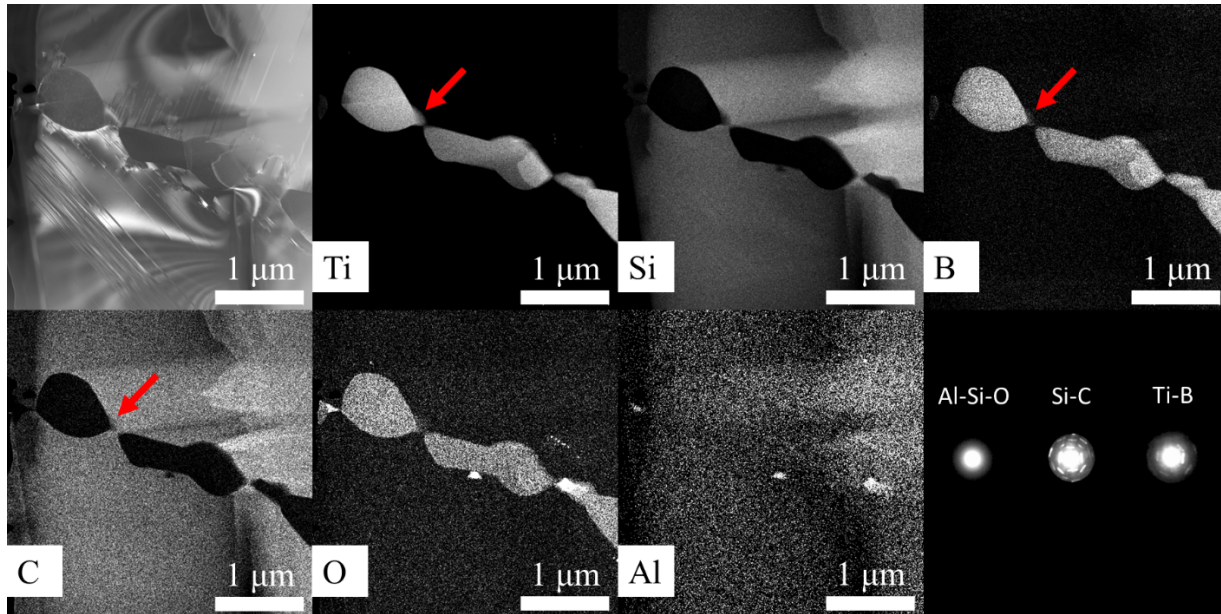


Figure 9: STEM image, EDS maps of the elements present, and pole figures of phases.

Figure 10 shows Raman Spectroscopy of the sample processed with precursor SiC and 60 MPa. Two patterns are identifiable as TiB_2 and SiC phases, but the third phase is not fully identifiable but has two peaks close to that of SiC and one amorphous peak at 1087 cm^{-1} that is either the Al-Si-O amorphous phase or unreacted B_4C . Aluminosilicate has a peak around 1070 cm^{-1} [29], which is close to that peak. In terms of all the individual precursor constituents, this peak most closely matches with B_4C , which has a peak around $1086\text{-}1088\text{ cm}^{-1}$ [30], [31]. This is intuitive because the boron is the fastest diffusing element, so it diffuses into the TiC and is held up by the TiB_2 layer formed. At the end of reaction, there could be some B_4C or B_xC system in grains or at grain boundaries of TiB_2 . The Raman peak at 1087 cm^{-1} is most likely from both the aluminosilicate, which is a contaminant from the materials and processing, and from small amounts of unreacted B_4C . The unreacted phase is not TiC. These are in such small amounts, but they contribute to the processing and properties.

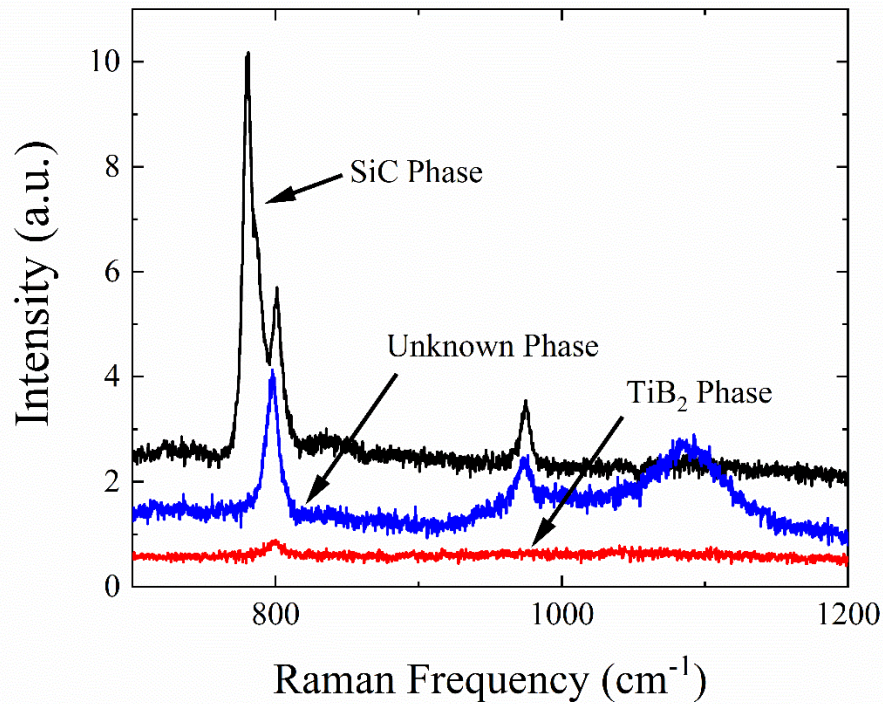


Figure 10: Raman spectra of the sample processed with precursor SiC and 60 MPa.

Table 2: Density, hardness, and fracture toughness values of composites.

Property	No precursor SiC and 30 MPa (direct comparison with hot pressing)	With precursor SiC and 30 MPa	With precursor SiC and 45 MPa	With precursor SiC and 60 MPa
Density (g/cm ³)	3.0 ± 0.1	3.58 ± 0.1	3.62 ± 0.1	3.66 ± 0.1
Density (%TD)	80 ± 1.1	95 ± 1.0	97 ± 1.1	99 ± 0.9
Hardness (GPa)	--	24.1 ± 1.4	24.6 ± 1.4	26.4 ± 1.3
Fracture Hardness (MPa m ^{1/2})	--	4.67 ± 0.4	4.83 ± 0.3	5.12 ± 0.2

Figure 11 shows SEM images of a typical indent used to measure Vickers microhardness and Palmquist indentation fracture toughness and the resulting propagating crack from the sample processed with 60 MPa and precursor SiC. The cracks extending from indents allow for measurement of Palmquist indentation fracture toughness [32]–[34]. Table 2 lists values for the hardness and fracture toughness of the composites processed with precursor SiC. The hardness and fracture toughness are slightly lower than hot pressed SiC-TiB₂ composite with no precursor SiC [21]. The cracks show three modes of propagation including crack deflection, crack bridging, and transgranular cracks through SiC particles. The two modes of crack propagation that improve the fracture toughness in the current research are the crack deflection around precursor SiC particles and newly formed SiC as well as crack bridging in the newly formed SiC.

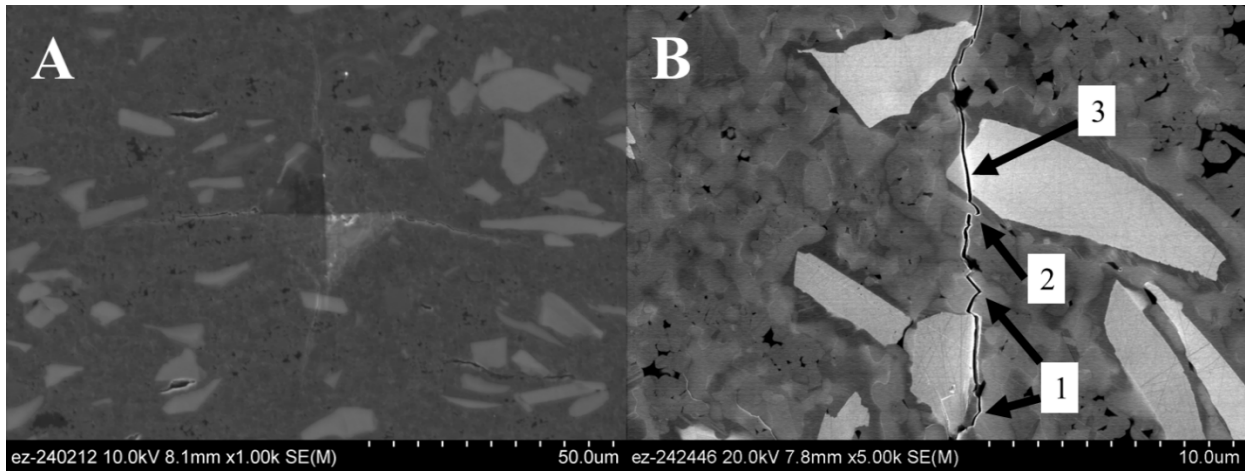


Figure 11: SEM image in secondary electron mode of A) a typical indentation resulting from Vickers hardness testing of a SiC-TiB₂ composite processed with 60 MPa and precursor SiC and B) resulting propagating crack. 1 is crack deflection, 2 is crack bridging, and 3 is a transgranular crack.

Discussion

The kinetics of the displacement reaction was not directly measured, but it is evident that the reactions of both powder blends mixed according to Eqs. (1) and (2) reacted fast enough to fully convert to reaction-bonded composites in SPS/FAST according to XRD. The DTA of the two powder blends suggests that the reactions occur slowly, but the heating rates in SPS/FAST are much higher compared to typical DTA heating rates. Furthermore, the density of the composite without precursor SiC was unexpectedly low compared to literature results with hot pressing, and the densification slowed at 1,400°C and then sharply increased at 1,700°C indicating that liquid Si aids in the densification and most likely the diffusion of C. A direct comparison between SPS/FAST and hot pressing was performed using alumina, and the study served as useful information for a non-reacting system [35]. A reacting system, like the one in the current research, is more complicated.

The addition of SiC as a precursor was needed for higher density with SPS/FAST processing, but the mechanism is not well understood. The densification of the composites with SiC precursor all increased gradually and became highly dense near 1,700°C. This could be because the addition of SiC allows for absorption of heat and ultimately a lower adiabatic temperature, or lower temperature to reach full reaction conversion. According to FactSage [36], Eq. (1) has higher adiabatic temperature compared to Eq. (2) (see Table 3). This was calculated based on Eq. (4), which solves Eq. (3) for the adiabatic condition, where $H_i(T)$ is the enthalpy of a component, $\Delta H_{f,i}^\circ$ is the heat of formation, $C_{p,i}$ is the heat capacity, $\Delta H_{s,i}$ is the heat of s'th phase transition, and n_i is the number of moles [37]. The adiabatic temperature is calculated from the reference temperature of 25°C.

Table 3 and Eq. (4) show that the adiabatic temperature must decrease when SiC precursor is added because the heat of formation plus the summation of the heat capacities of products must equal zero and by adding SiC precursor, the SiC on the product side will be increased from 3 to 4. This makes sense physically because the SiC absorbs energy, and it makes sense mathematically as mentioned above where n_i is increased. The final enthalpies are also reported in Table 3. The final enthalpy is less negative for Eq. (1) suggesting that less energy was released and thus higher adiabatic temperature. It also means that the samples processed with precursor SiC have a final thermodynamic state that has higher enthalpy, or more energy to release heat or work because the SiC particles absorbed it.

$$H_i(T) = \Delta H_{f,i}^{\circ} + \int_{T_0}^T C_{p,i} dT + \sum \Delta H_{s,i} \quad (3)$$

$$0 = \Delta H_{f,i}^{\circ} + \sum_{\text{Products}} n_i \int_{25^{\circ}\text{C}}^{T_{\text{adiabatic}}} C_{p,i} dT \quad (4)$$

In the current research, where composites were processed according to Eqs. (1) and (2) and at the same heating rates, the powder blend without SiC might proceed to completion before the blend with SiC added as a precursor because the SiC can absorb the energy and decrease the reaction rate. The blend without SiC precursor will most likely fully convert to SiC-TiB₂ before the blend with SiC precursor. This is most likely why the densification seemed to slow around 1,400°C; the TiB₂ phase had progressed in formation, then the densification increases after 1500, which is most likely from the Si melting and enhancing the formation of TiB₂ as well as form SiC. Further densification or consolidation continued toward the end of the heating cycle, but it was most likely the result of grain-boundary sliding and particle fracture, and hence, the low density observed. Because the densification curve of the powder blends with SiC precursor slowly reached high densities, it was most likely from a slower reaction because of energy absorption through the SiC precursor particles. Then the density could be further increased with added pressure, where pressure effects kept the materials close together while the reactions completed in the confined volume, and diffusion is enhanced by Coble creep mechanisms [38]–[40].

The microstructure consists of the larger precursor SiC particles amongst reaction bonded SiC-TiB₂. The SiC that formed during processing is the matrix, and the TiB₂ that formed was the reinforcement inside the SiC matrix. There is nearly 100% conversion to the product side of Eq. (2), and the different colored TiB₂ grains are most likely differently oriented grains. The TEM shows that there are no other bulk phases except for SiC and TiB₂. There are very small amounts of unreacted B₄C and a contaminant Al-Si-O amorphous phase.

The mechanical properties in terms of Vickers microhardness and fracture toughness are high compared to the individual constituents, which is improved from the reaction bonding process. The fracture toughness is higher than pure SiC but lower than TiB₂ [10]. The hardness values are closer to that of SiC [41]. However, the fracture toughness and hardness are slightly lower

compared to [21], which is because our material has higher SiC content and more interfaces due to the addition of SiC precursor.

Table 3: Reaction thermodynamics for combustion reactions of both powder blends according to Eqs. (1) and (2) starting at room temperature, $T_0 = 25^\circ\text{C}$.

Equation	Enthalpy of Formation at 25°C , ΔH_R (kJ)	Final Enthalpy of Reaction, H (kJ)	Adiabatic Combustion Temperature, T_a ($^\circ\text{C}$)
(1)	-349.31	-430.90	1,258
(2)	-349.31	-502.45	1,115

Conclusion

Fully dense displacement reaction-bonded SiC-TiB₂ composites were synthesized using B₄C, TiC, Si and SiC as precursor powders and SPS/FAST processing. It was found that it is possible to achieve very high densification, as large as 99%, with very short processing times when using SPS/FAST. It was also found that when SiC was not used as a precursor, bodies with only 80% density were obtained. Additional applied pressure in the system processed with a SiC precursor resulted in a fully dense composite with higher SiC content, which lowered the theoretical density of the composite. The addition of SiC is thought to decrease the reaction rate by absorbing energy from the exotherm. Vickers hardness and fracture toughness of the composite with the highest density was near 26 GPa and 5.12 MPa m^{1/2}, respectively. Cracks emanating from the corners of the indent propagated through and around phases of SiC and around TiB₂ phase. By using SPS/FAST for synthesis, the throughput for this material can be increased for applications that desire high hardness and fracture toughness as in armor.

Acknowledgments

Corson L. Cramer would like to thank Walter Koncinski for help formatting and editing. This material is based upon work supported by the U.S. Department of Energy, Office of Energy Efficiency and Renewable Energy, Office of Advanced Manufacturing and Propulsion Materials program under the Vehicle Technology Office, under contract number DE-AC05-00OR22725.

References

- [1] D. Demirskyi, J. Cheng, D. Agrawal, and A. Ragulya, "Densification and grain growth during microwave sintering of titanium diboride," *Scr. Mater.*, vol. 69, no. 8, pp. 610–613, Oct. 2013.
- [2] B. Basu, G. B. Raju, and A. K. Suri, "Processing and properties of monolithic TiB₂ based materials," *Int. Mater. Rev.*, vol. 51, no. 6, pp. 352–374, Dec. 2006.
- [3] R. Maboudian, C. Carraro, D. G. Senesky, and C. S. Roper, "Advances in silicon carbide science and technology at the micro- and nanoscales," *J. Vac. Sci. Technol. A Vacuum, Surfaces, Film.*, vol. 31, no. 5, p. 050805, Sep. 2013.
- [4] D. S. King, W. G. Fahrenholtz, and G. E. Hilmas, "Microstructural Effects on the Mechanical

- Properties of SiC-15 vol% TiB₂ Particulate-Reinforced Ceramic Composites,” *J. Am. Ceram. Soc.*, p. n/a-n/a, Nov. 2012.
- [5] S. Ran, O. Van der Biest, and J. Vleugels, “In situ platelet-toughened TiB₂-SiC composites prepared by reactive pulsed electric current sintering,” *Scr. Mater.*, vol. 64, no. 12, pp. 1145–1148, Jun. 2011.
- [6] O. O. Ajayi, A. Erdemir, R. H. Lee, and F. A. Nichols, “Sliding Wear of Silicon Carbide-Titanium Boride Ceramic-Matrix Composite,” *J. Am. Ceram. Soc.*, vol. 76, no. 2, pp. 511–517, Feb. 1993.
- [7] C. GRESKOVICH and J. H. ROSOLOWSKI, “Sintering of Covalent Solids,” *J. Am. Ceram. Soc.*, vol. 59, no. 7–8, pp. 336–343, Jul. 1976.
- [8] E. Gomez, J. Echeberria, I. Iturriza, and F. Castro, “Liquid phase sintering of SiC with additions of Y₂O₃, Al₂O₃ and SiO₂,” *J. Eur. Ceram. Soc.*, vol. 24, no. 9, pp. 2895–2903, Aug. 2004.
- [9] G. . Zhang, X. . Yue, Z. . Jin, and J. . Dai, “In-situ synthesized TiB₂ toughened SiC,” *J. Eur. Ceram. Soc.*, vol. 16, no. 4, pp. 409–412, Jan. 1996.
- [10] Y. Ohya, M. J. Hoffmann, and G. Petzow, “Sintering of in-Situ Synthesized SiC-TiB₂ Composites with Improved Fracture Toughness,” *J. Am. Ceram. Soc.*, vol. 75, no. 9, pp. 2479–2483, Sep. 1992.
- [11] D. S. King, W. G. Fahrenholtz, and G. E. Hilmas, “Silicon carbide-titanium diboride ceramic composites,” *J. Eur. Ceram. Soc.*, vol. 33, no. 15–16, pp. 2943–2951, Dec. 2013.
- [12] D. Bucevac, B. Matovic, S. Boskovic, S. Zec, and V. Krstic, “Pressureless sintering of internally synthesized SiC-TiB₂ composites with improved fracture strength,” *J. Alloys Compd.*, vol. 509, no. 3, pp. 990–996, Jan. 2011.
- [13] T. Tani and S. Wada, “SiC matrix composites reinforced with internally synthesized TiB₂,” *J. Mater. Sci.*, vol. 25, no. 1, pp. 157–160, Jan. 1990.
- [14] G. J. Zhang, Z. Z. Jin, and X. M. Yue, “Reaction synthesis of TiB₂-SiC composites from TiH₂-Si-B₄C,” *Mater. Lett.*, vol. 25, no. 3–4, pp. 97–100, Nov. 1995.
- [15] G. J. Zhang, Z. Z. Jin, and X. M. Yue, “TiB₂-Ti(C, N)-SiC composites prepared by reactive hot pressing,” *J. Mater. Sci. Lett.*, vol. 15, no. 1, pp. 26–28, Jan. 1996.
- [16] D. A. Hoke, D. K. Kim, J. C. LaSalvia, and M. A. Meyers, “Combustion Synthesis/Dynamic Densification of a TiB₂-SiC Composite,” *J. Am. Ceram. Soc.*, vol. 79, no. 1, pp. 177–182, Jan. 1996.
- [17] D. Vallauri, I. C. Atías Adrián, and A. Chrysanthou, “TiC-TiB₂ composites: A review of phase relationships, processing and properties,” *J. Eur. Ceram. Soc.*, vol. 28, no. 8, pp. 1697–1713, Jan. 2008.
- [18] D. Brodtkin, S. R. Kalidindi, M. W. Barsoum, and A. Zavaliangos, “Microstructural Evolution during Transient Plastic Phase Processing of Titanium Carbide-Titanium Boride Composites,” *J. Am. Ceram. Soc.*, vol. 79, no. 7, pp. 1945–1952, Jul. 1996.
- [19] G. Zhao, C. Huang, H. Liu, B. Zou, H. Zhu, and J. Wang, “Microstructure and mechanical properties of TiB₂-SiC ceramic composites by Reactive Hot Pressing,” *Int. J. Refract. Met. Hard Mater.*, vol. 42, pp. 36–41, Jan. 2014.
- [20] G. Zhao, C. Huang, H. Liu, B. Zou, H. Zhu, and J. Wang, “A study on in-situ synthesis of TiB₂-SiC ceramic composites by reactive hot pressing,” *Ceram. Int.*, vol. 40, no. 1, pp. 2305–2313, Jan.

- 2014.
- [21] Z. Zhang *et al.*, "Synthesis mechanism and mechanical properties of TiB₂-SiC composites fabricated with the B₄C-TiC-Si system by reactive hot pressing," *J. Alloys Compd.*, vol. 619, pp. 26-30, Jan. 2015.
- [22] X. Zhang *et al.*, "Effects of particle size of raw materials on the characteristics of TiB₂-SiC composites fabricated from B₄C, TiC and Si powders," *Ceram. Int.*, Sep. 2018.
- [23] O. Guillon *et al.*, "Field-Assisted Sintering Technology/Spark Plasma Sintering: Mechanisms, Materials, and Technology Developments," *Adv. Eng. Mater.*, vol. 16, no. 7, pp. 830-849, Jul. 2014.
- [24] A. M. Locci, R. Orru, G. Cao, and Z. A. Munir, "Simultaneous Spark Plasma Synthesis and Densification of TiC-TiB₂ Composites," *J. Am. Ceram. Soc.*, vol. 89, no. 3, pp. 848-855, Mar. 2006.
- [25] J. Zhang, L. Wang, L. Shi, W. Jiang, and L. Chen, "Rapid fabrication of Ti₃SiC₂-SiC nanocomposite using the spark plasma sintering-reactive synthesis (SPS-RS) method," *Scr. Mater.*, vol. 56, no. 3, pp. 241-244, Feb. 2007.
- [26] Z. A. Munir, D. V. Quach, and M. Ohyanagi, "Electric Current Activation of Sintering: A Review of the Pulsed Electric Current Sintering Process," *J. Am. Ceram. Soc.*, vol. 94, no. 1, pp. 1-19, Jan. 2011.
- [27] "Microstructural evolution during silicon carbide (SiC) formation by liquid silicon infiltration using optical microscopy," *Int. J. Refract. Met. Hard Mater.*, vol. 28, no. 2, pp. 191-197, Mar. 2010.
- [28] G. Zhu *et al.*, "Formation Mechanism of Spherical TiC in Ni-Ti-C System during Combustion Synthesis," *Materials (Basel)*, vol. 10, no. 9, p. 1007, Aug. 2017.
- [29] Y. Yu, G. Xiong, C. Li, and F.-S. Xiao, "Characterization of aluminosilicate zeolites by UV Raman spectroscopy," *Microporous Mesoporous Mater.*, vol. 46, no. 1, pp. 23-34, Jul. 2001.
- [30] K. M. Reddy, P. Liu, A. Hirata, T. Fujita, and M. W. Chen, "Atomic structure of amorphous shear bands in boron carbide," *Nat. Commun.*, vol. 4, no. 1, p. 2483, Dec. 2013.
- [31] J. Guo, L. Zhang, T. Fujita, T. Goto, and M. Chen, "Pressure-induced depolarization and resonance in Raman scattering of single-crystalline boron carbide," *Phys. Rev. B*, vol. 81, no. 6, p. 060102, Feb. 2010.
- [32] D. K. Shetty, I. G. Wright, P. N. Mincer, and A. H. Clauer, "Indentation fracture of WC-Co cermets," *J. Mater. Sci.*, vol. 20, pp. 1873-1882.
- [33] S. Sheikh *et al.*, "Fracture toughness of cemented carbides: Testing method and microstructural effects," *Int. J. Refract. Met. Hard Mater.*, no. 8.
- [34] P. CHANTIKUL, G. R. ANSTIS, B. R. LAWN, and D. B. MARSHALL, "A Critical Evaluation of Indentation Techniques for Measuring Fracture Toughness: II, Strength Method," *J. Am. Ceram. Soc.*, vol. 64, no. 9, pp. 539-543, Sep. 1981.
- [35] J. Langer, M. J. Hoffmann, and O. Guillon, "Direct comparison between hot pressing and electric field-assisted sintering of submicron alumina," *Acta Mater.*, vol. 57, no. 18, pp. 5454-5465, Oct. 2009.
- [36] C. W. Bale *et al.*, "FactSage thermochemical software and databases," *Calphad*, vol. 26, no. 2, pp.

189–228, Jun. 2002.

- [37] A. Varma, A. S. Rogachev, A. S. Mukasyan, and S. Hwang, “Combustion Synthesis of Advanced Materials: Principles and Applications,” *Adv. Chem. Eng.*, vol. 24, no. C, pp. 79–226, 1998.
- [38] R. L. Coble, “A Model for Boundary Diffusion Controlled Creep in Polycrystalline Materials,” *J. Appl. Phys.*, vol. 34, no. 6, pp. 1679–1682, Jun. 1963.
- [39] D. A. Krohn, P. A. Urick, D. P. H. Hasselman, and T. G. Langdon, “Evidence for Coble creep in the relaxation of surface-compressive stresses in tempered polycrystalline aluminum oxide,” *J. Appl. Phys.*, vol. 45, no. 9, pp. 3729–3731, Sep. 1974.
- [40] R. D. Nixon and R. F. Davis, “Diffusion-Accommodated Grain Boundary Sliding and Dislocation Glide in the Creep of Sintered Alpha Silicon Carbide,” *J. Am. Ceram. Soc.*, vol. 75, no. 7, pp. 1786–1795, Jul. 1992.
- [41] L. Vargas-Gonzalez, R. F. Speyer, and J. Campbell, “Flexural Strength, Fracture Toughness, and Hardness of Silicon Carbide and Boron Carbide Armor Ceramics,” *Int. J. Appl. Ceram. Technol.*, vol. 7, no. 5, pp. 643–651, Feb. 2010.